Inorganic Chemistry

ARTICLE

pubs.acs.org/IC

Cyano-bridged Homodinuclear Copper(II) Complexes

Mihail Atanasov,[*,†,§,∥] Peter Comba,[*,†] Graeme R. Hanson,[‡] Sascha Hausberg,[†] Stefan Helmle,[†] and Hubert Wadepohl[†]

[†]Universität Heidelberg, Anorganisch-Chemisches Institut, D-69120 Heidelberg, Germany

[‡]Centre for Advanced Imaging, The University of Queensland, Brisbane, Queensland 4072, Australia

[§]Institute of General and Inorganic Chemistry, Bulgarian Academy of Sciences, Acad.Georgi Bontchev Str. Bl.11, 1113 Sofia, Bulgaria

[∥]Institute for Physical and Theoretical Chemistry, University of Bonn, Wegelerstrasse 12, D-53115 Bonn, Germany

Supporting Information

ABSTRACT: The synthesis and structural analysis (single crystal X-ray data) of two mononuclear ($[Cu(L^1)(CN)]BF_4$ and $[Cu(L^3)(CN)](BF_4)$) and three related, cyanide-bridged homodinuclear complexes ($[\{Cu(L^1)\}_2(CN)](BF_4)_3 \cdot 1.35\ H_2O$, $[\{Cu(L^2)\}_2(CN)](BF_4)_3$ and $[\{Ni(L^3)\}_2(CN)](BF_4)_3$) with a tetradentate ($L^1$) and two isomeric pentadentate bispidine ligands (L^2, L^3; bispidines are 3,7-diazabicyclo-[3.3.1]nonane derivatives) are reported, together with experimental magnetic, electron paramagnetic resonance (EPR), and electronic spectroscopic data and a ligand-field-theory-based analysis. The temperature dependence of the magnetic susceptibilities and EPR transitions of the dicopper(II) complexes, together with the simulation of the EPR spectra of the mono- and dinuclear complexes leads to an anisotropic set of *g*- and *A*-values, zero-field splitting (ZFS) and magnetic exchange parameters (Cu1: $g_z = 2.055$, $g_x = 2.096$, $g_y = 2.260$, $A_z = 8$, $A_x = 8$, $A_y = 195 \times 10^{-4}\ cm^{-1}$, Cu2: g and A as for Cu_1 but rotated by the Euler angles $\alpha = -6°$, $\beta = 100°$, $D_{exc} = -0.07\ cm^{-1}$, $E_{exc}/D_{exc} = 0.205$ for $[\{Cu(L^1)\}_2(CN)](BF_4)_3 \cdot 1.35\ H_2O$; Cu1,2: $g_z = 2.025$, $g_x = 2.096$, $g_y = 2.240$, $A_z = 8$, $A_x = 8$, $A_y = 190 \times 10^{-4} cm^{-1}$, $D_{exc} = -0.159\ cm^{-1}$, $E_{exc}/D_{exc} = 0.080$ for $[\{Cu(L^2)\}_2(CN)](BF_4)_3$). Thorough ligand-field-theory-based analyses, involving all micro states and all relevant interactions (Jahn−Teller and spin−orbit coupling) and DFT calculations of the magnetic exchange leads to good agreement between the experimental observations and theoretical predictions. The direction of the symmetric magnetic anisotropy tensor $\boldsymbol{D}_{exc}$ in $[\{Cu(L^2)\}_2(CN)](BF_4)_3$ is close to the Cu···Cu vector (22°), that is, nearly perpendicular to the Jahn−Teller axis of each of the two Cu^{II} centers, and this reflects the crystallographically observed geometry. Antisymmetric exchange in $[\{Cu(L^1)\}_2(CN)](BF_4)_3 \cdot 1.35\ H_2O$ causes a mixing between the singlet ground state and the triplet excited state, and this also reflects the observed geometry with a rotation of the two Cu^{II} sites around the Cu···Cu axis.

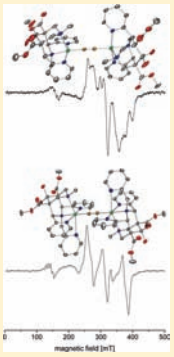

INTRODUCTION

A wide range of dicopper(II) complexes have been investigated since the discovery and extensive study of the dinuclear Cu^{II} carboxylates in the 1950s.[1−3] Among the large group of dicopper(II) complexes, there are only few with cyanide bridges, and this is partially due to the propensity of cyanide to reduce Cu^{II} with the oxidation of cyanide to cyanogens.[4] A model for the magnetic exchange through cyanide bridges has been developed and used to analyze spin delocalization and spin polarization across the CN^- bridge of cyanometalates with Cu^{II}-NC-M^{III} fragments,[5] and a ligand-field-theory-based quantum-chemical model has been developed[6] and used to analyze a series of trinuclear cyanometalates.[7] Recent work on Cu^{II}-X-Cu^{II} systems (X = halogenide,[8] CN^-[9]), supported by a DFT-based analysis, has demonstrated the important role of the type of bonding involving the Cu^{II} centers, the variation of the Cu^{II}-X-Cu^{II} geometry, and the nature of the terminal ligands. Therefore, a simple homodinuclear system with coupled t_{2g}^6-e_g^3 Cu^{II} sites is an interesting target to thoroughly study the exchange interaction based on spectroscopy (electron paramagnetic resonance (EPR) and electronic spectroscopies) and magnetism, combined with experimental and computational structural studies.

A detailed analysis of the coupling of the electronic states of a simple homodinuclear system is also of interest in the field of single-molecule magnetism (SMM), a phenomenon discovered at the beginning of the 1990s.[10,11] A large number of these fascinating types of molecules has been reported, but only little progress has been made to increase the energy barrier to magnetization relaxation [$U_{eff} \propto S^2 D$; spin *S*, zero-field splitting (ZFS) *D*], and so far there are only very few molecular compounds which are magnets at significantly higher than liquid He temperatures. In recent years, there has been much progress in understanding and in the computation of isotropic and anisotropic exchange coupling parameters,[12−14] but for large oligonuclear metal complexes, it is still difficult to extract a unique set of exchange coupling constants from experimental data, and computational studies are hampered by the large number of possible solutions. However, the major problem in developing higher temperature SMMs is a limited understanding of the local single ion and the total magnetic anisotropies *D* and their dependence on

Received: December 6, 2010
Published: June 28, 2011

Chart 1. Structure and Numbering of the Ligands Used

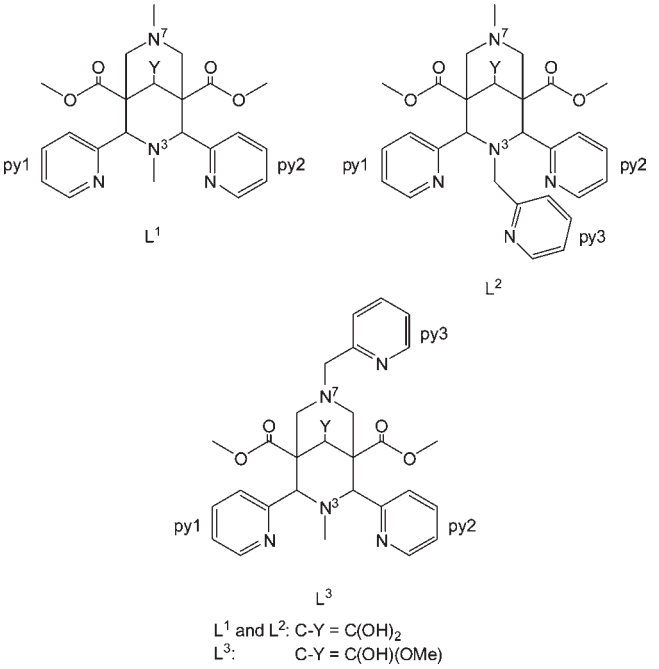

the local and global geometries.[15−19] The fundamental relation between the ZFS D and the total spin S[20,21] as well as the recent discovery of relatively small oligonuclear and of mononuclear complexes with SMM behavior[22,23] are good reasons for a detailed analysis of the electronics of simple exchange-coupled systems.

Herein, we therefore report the electronic properties of two cyanide-bridged homodinuclear Cu^{II} complexes, coordinated to thoroughly studied bispidine ligand systems,[24] that is, the tetradentate bispidine L^1 [25] and a pentadentate bispidine L^2 (bispidines are 3,7-diazabicyclo[3.3.1]nonane, see Chart 1 for the structures of L^1, L^2, and L^3),[26] which enforce a rigid Cu^{II} coordination geometry, with the cyanide bridge aligned perpendicular to the pseudo-Jahn−Teller axes for the two Cu^{II} ions.[24,27−29] A cyanide-bridged homodinuclear Ni^{II} complex with the pentadentate bispidine L^3, an isomer of L^2, and the corresponding mononuclear Cu^{II} complexes are also reported. The isotropic and anisotropic exchange coupling pathways and parameters are analyzed on the basis of the experimental and computed structures, as well as the experimental spectroscopic (EPR and electronic spectra) and magnetic data.

Magnetic anisotropy in dicopper(II) complexes has been studied extensively by EPR spectroscopy, and the interplay between ligand fields, superexchange, and spin−orbit coupling was generally analyzed by perturbation theory.[30−37] Universal theoretical approaches to extract anisotropic spin-Hamiltonian parameters based on DFT[6,38,39] and correlated ab initio calculations[40−42] have been described. However, because of the size of the dinuclear systems considered here, these approaches are prohibitive. Therefore, a microscopic ligand field approach is used to obtain its parameters from spectroscopic and magnetic data to analyze the origin of the magnetic anisotropy in these systems.

RESULTS AND DISCUSSION

Syntheses and Structural Properties. The reaction of $[Cu(L^1)(CN)]BF_4$ with $[Cu(L^1)](BF_4)_2$ or of $[Cu(L^2)](BF_4)_2$ with NaCN, produced the two homodinuclear cyanide-bridged Cu^{II} complexes $[\{Cu(L^1)\}_2(CN)](BF_4)_3\cdot 1.35H_2O$ and $[\{Cu(L^2)\}_2(CN)](BF_4)_3$. The homodinuclear Ni^{II} complex $[\{Ni(L^3)\}_2(CN)](BF_4)_3$ was also prepared in moderate yield. From the reaction of $[Cu(L^3)](BF_4)_2$ with tetraethylammonium cyanide, only the mononuclear complex $[Cu(L^3)(CN)]BF_4$ was isolated. Single crystals of the L^1-based mononuclear cyanide complex were also analyzed. ORTEP plots of all experimentally determined structures appear in Figure 1, and selected structural data are listed in Table 1.

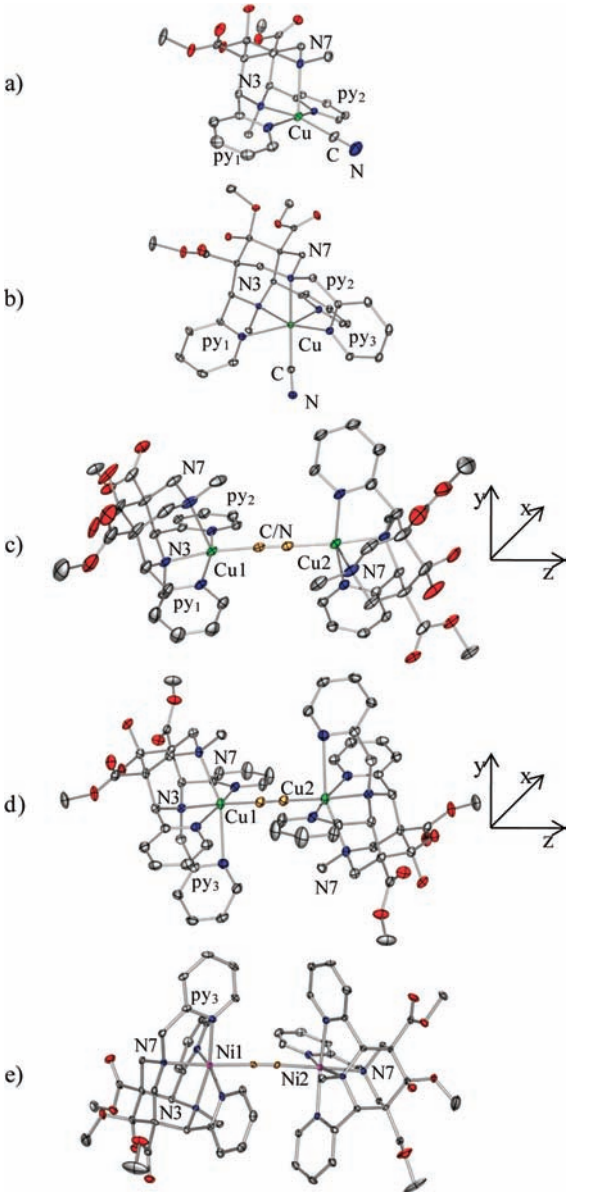

Figure 1. Plots of the molecular cations of the X-ray structures of (a) $[Cu(L^1)(CN)]^+$, (b) $[Cu(L^3)(CN)]^+$, (c) $[\{Cu(L^1)\}_2(CN)]^{3+}$, (d) $[\{Cu(L^2)\}_2(CN)]^{3+}$, and (e) $[\{Ni(L^3)\}_2(CN)]^{3+}$ showing 30% probability ellipsoids and the atom labeling. Hydrogen atoms have been omitted for clarity.

The characteristic structural data of the mono- and dinuclear bispidine complexes are all in the expected range (specifically also the N3···N7 distances (2.86 Å−2.92 Å) and the M−N bond lengths).[24,27,43] With the exception of the mononuclear

dx.doi.org/10.1021/ic102430a |Inorg. Chem. 2011, 50, 6890–6901

Table 1. Selected Structural Data[a] of $[\{Cu(L^1)\}_2(CN)](BF_4)_3 \cdot 1.35H_2O$, $[\{Cu(L^2)\}_2(CN)](BF_4)_3$, $[Cu(L^1)(CN)]BF_4$, $[Cu(L^3)(CN)]BF_4$, and $[\{Ni(L^3)\}_2(CN)](BF_4)_3$

	$[\{Cu(L^1)\}_2(CN)](BF_4)_3 \cdot 1.35H_2O$	$[\{Cu(L^2)\}_2(CN)](BF_4)_3$	$[Cu(L^1)(CN)]BF_4$	$[Cu(L^3)(CN)]BF_4$	$[\{Ni(L^3)\}_2(CN)](BF_4)_3$[b]
			Distances [Å]		
M[c]–N(3)	2.013(4)	2.037(3)	2.026(3)	2.133(2)	2.098(4), 2.097(4)
M–N(7)	2.295(4)	2.385(3)	2.250(3)	2.083(2)	2.170(3), 2.179(3)
$M–N_{py1}$	2.007(4)	2.023(3)	1.997(3)	2.381(2)	2.062(4), 2.062(4)
$M–N_{py2}$	1.998(4)	1.993(3)	2.006(3)	2.383(2)	2.132(4), 2.117(4)
$M–N_{py3}$	(2.99)[d]	2.598(3)		2.020(2)	2.052(4), 2.071(4)
M–C/N[e]	1.948(4)	1.971(4)	1.933(4)[f]	1.983(2)[f]	2.047(4), 2.062(4)
C–N	1.162(9)	1.148(7)	1.137(5)	1.150(3)	1.171(7), 1.118(7)
M1···M2	5.053(1)	5.091(1)			5.265(3), 5.240(3)
			Angles [deg]		
M–C–N/N–C	176.6(2)	178.8(5)	178.8(4)	176.2(2)	178.7(3), 177.9(3)
N(3)–M–C/N	171.6(2)	176.6(1)	167.7(1)	98.15(7)	98.5(1), 99.0(2)
N(7)–M–C/N	103.9(2)	101.2(1)	107.4(1)	175.29(7)	176.1(2), 175.0(2)
N_{py1}–M–C/N	97.3(2)	97.2(1)	97.4(1)	87.74(7)	89.4(2), 89.0(2)
N_{py2}–M–C/N	98.1(2)	97.7(1)	97.2(1)	89.34(7)	87.4(1), 88.1(2)
N_{py3}–M–C/N		97.6(1)		93.82(7)	93.9(2), 93.8(2)

[a] Distances in Å, angles in deg, with estimated standard deviations in parentheses. [b] Since there are two crystallographic independent structures in the unit cell, two values are given for each bond and angle. [c] M = Cu or Ni. [d] Weakly bonded to a fluorine atom of the counterion tetrafluoroborate. [e] Since the cyanide is disordered, only an average distance is given. [f] The copper(II) is C-bonded to the cyanide ligand.

Cu^{II} complex of L^3, all Cu^{II} complexes have an elongation along the N7–Cu bond, perpendicular to the CN^- bridge. The change of direction of the pseudo-Jahn–Teller axis in the Cu^{II} complex of L^3 (elongation along the py1-Cu-py2 axis) is the result of the strong ligand field induced by the CN^- ligand, which leads to a destabilization of the geometry with a pseudo-Jahn–Teller axis along N7–Cu–CN.[7] All three possible tetragonally elongated isomeric structures have been observed with bispidine-Cu^{II} complexes,[28,29], namely, a switch between various distortional isomers is not unexpected.

$[Cu(L^1)(CN)]BF_4$. The Cu^{II} complex with the tetradentate bispidine has a square-based pyramidal structure, with CN^- coordinated in the xy plane (*trans* to N3) and a long bond to the apical N7 donor.

$[Cu(L^3)(CN)]BF_4$. There are two remarkable but not unexpected differences between this structure with a pentadentate bispidine and the structure above with the tetradentate bispidine L^1: the pseudo-Jahn–Teller axis is along the py1-Cu-py2 axis (i.e., it is perpendicular to the strong CN^- ligand), and the Cu–CN bond (1.983 Å) is significantly longer and therefore weaker than in $[Cu(L^1)(CN)]BF_4$ (1.933 Å). We have not been able to trap and isolate a CN^- bridged dicopper(II) complex with L^3, and the observed structural characteristics suggest that this might be for thermodynamic reasons.

$[\{Cu(L^1)\}_2(CN)](BF_4)_3 \cdot 1.35\ H_2O$ and $[\{Cu(L^2)\}_2(CN)](BF_4)_3$. The structural parameters of specific interest for magnetic exchange between the two Cu^{II} centers are (i) the linearity of the CN^- bridge (Cu1–C–N, C–N–Cu2),[9] (ii) the Cu···Cu distance, and (iii) the orthogonality of the magnetic orbitals, which depends on the relative orientation of the two Cu^{II} sites.[44] In our dinuclear complexes, the two Cu^{II} centers are nearly linearly bridged (Cu–C–N/N–C angles of 176.6° and 178.8°). Interestingly, the two Cu^{II} subunits in $[\{Cu(L^1)\}_2(CN)](BF_4)_3 \cdot 1.35\ H_2O$ are twisted about the Cu-CN/NC-Cu axis with a torsion angle N7–Cu···Cu–N7 of 87.2°, whereas the corresponding torsion angle in $[\{Cu(L^2)\}_2(CN)](BF_4)_3$ is 180°, and this is the most significant structural difference between the two dicopper(II) structures (see Figure 1). In both complexes the pseudo-Jahn–Teller axis is, as expected, perpendicular to the CN^- bridge, that is, along the Cu–N7 bond (on the same axis there is a weak interaction to a BF_4^- ion (2.99 Å) in the L^1-based complex and to a pyridine group (2.60 Å) in the L^2-based complex). There are significant differences in the Cu–C/N, the C–N, and, therefore, the Cu···Cu distances, between the two complexes. The two major structural differences, that is, the distances and torsion angles along the cyanide bridge, are expected to lead to significant differences in the electronic and magnetic behavior. The nearest intermolecular $Cu_2 \cdots Cu_2$ distances are 8.804 and 8.914 Å for $[\{Cu(L^1)\}_2(CN)](BF_4)_3 \cdot 1.35\ H_2O$ and $[\{Cu(L^2)\}_2(CN)](BF_4)_3$, respectively, and this is found to perturb the EPR spectra (vide infra).

$[\{Ni(L^3)\}_2(CN)](BF_4)_3$. This complex crystallizes with two essentially identical half-molecules in the asymmetric unit. The Ni^{II} centers are nearly linearly bridged with a Ni–C–N/N–C angle of 178.7° (177.9°). Only a few stable bispidine-Ni^{II} complexes are known,[24,45,46] and the Ni–N distances of the CN^- bridged dinickel(II) complex are in the expected range.[43,46] There is a twist around the Ni-CN/NC-Ni axis with an N3–Ni···Ni–N3 torsion angle of 106.2°/108.7°. The Ni-CN/NC bond distances are comparable to other known CN^- bridged dinickel(II) complexes.[9]

Spectroscopy and Magnetism. The IR spectra of the three dinuclear complexes have the characteristic CN stretching bands of cyanide-bridges.[47] For $[\{Cu(L^1)\}_2(CN)](BF_4)_3$ the ν(CN) band appears at 2182 cm^{-1}; as is typical for CN^- bridged dinuclear complexes,[9] it is shifted by 30 cm^{-1} to higher energy with respect to the corresponding mononuclear complex $[Cu(L^1)(CN)]BF_4$ (ν(CN) = 2152 cm^{-1}). For $[\{Cu(L^2)\}_2(CN)](BF_4)_3$ the ν(CN) peak is at slightly lower energy (2165 cm^{-1}), although a slightly shorter CN bond (0.038 Å) is apparent from

dx.doi.org/10.1021/ic102430a |*Inorg. Chem.* 2011, 50, 6890–6901

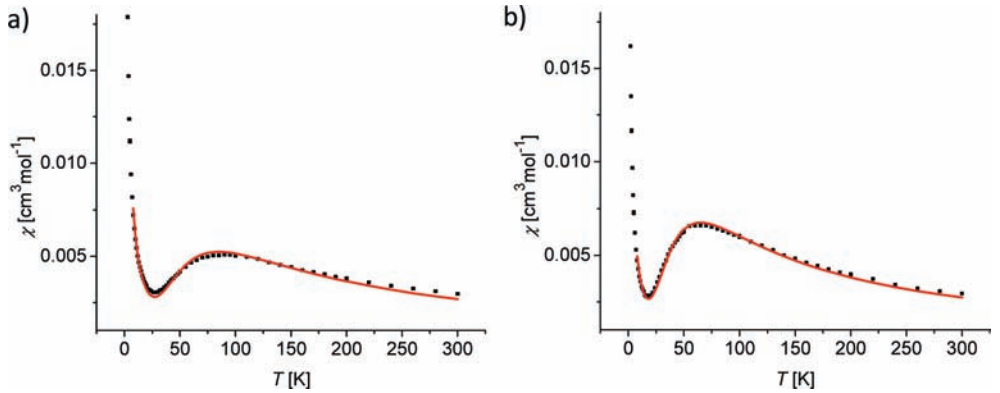

Figure 2. Magnetic susceptibility versus T for (a) $[\{Cu(L^1)\}_2(CN)](BF_4)_3 \cdot 1.35H_2O$ and (b) $[\{Cu(L^2)\}_2(CN)](BF_4)_3$ from experiment (black squares) and calculated from the Bleaney–Bowers fit, eq 1 (red line, see text).

the structural data (see Table 1). This is not unexpected since the C–N distance in cyanides is not significantly affected by geometric and/or electronic variations, for example, terminal or bridging CN^- anions generally have similar C–N distances.[4] For $[\{Ni(L^3)\}_2(CN)](BF_4)_3$ a broad band appears at 2150 cm^{-1}, and this is as expected from other cyanide-bridged dinickel(II) complexes.[9]

Magnetic susceptibility measurements were performed on powdered crystals of $[\{Cu(L^n)\}_2(CN)](BF_4)_3$ (n = 1,2) at 500 G in the temperature range of 2–300 K.[48] Plots of χ_M versus T have a maximum at around 80 and 65 K for $[\{Cu(L^1)\}_2(CN)](BF_4)_3$ and $[\{Cu(L^2)\}_2(CN)](BF_4)_3$, respectively, and the χ_M values slowly decrease at higher temperatures (see Figure 2); at temperatures below 15 K, there is a sharp increase of χ_M in both compounds, and this is due to a small impurity by the mononuclear complexes.[49,50] The general behavior of the susceptibility data is consistent with antiferromagnetic coupling between the two Cu^{II} ions with a local spin of $S = 1/2$. The room temperature χT values in both compounds are in the expected range for two uncoupled $S = 1/2$ spins (spin-only value of 0.75) with a g-value slightly larger than the g-factor of the free electron (i.e., χT (300 K) = 0.891 emu K mol^{-1} for $[\{Cu(L^1)\}_2(CN)](BF_4)_3$ and χT (300 K) = 0.885 emu K mol^{-1} for $[\{Cu(L^2)\}_2(CN)](BF_4)_3$). The susceptibility data were reproduced with a fit using the Bleaney–Bowers approach (eq 1),[2]

$$\chi = \frac{2Ng^2\beta^2}{kT(3 + e^{-J/kT})}(1 - \rho) + \frac{Ng^2\beta^2}{2kT}\rho + \chi_{TIP} \qquad (1)$$

based on the isotropic exchange spin Hamiltonian $H = -J\,\boldsymbol{S}_1 \cdot \boldsymbol{S}_2$ ($S_1 = S_2 = 1/2$), where ρ is the fraction of the Cu^{2+} impurity. The best fit of the experimental data is obtained with $J = -104.3$ cm^{-1}, g = 2.17, ρ = 0.0674 with R^2 = 0.967 for $[\{Cu(L^1)\}_2(CN)](BF_4)_3$, and $J = -76.5$ cm^{-1}, g = 2.15, ρ = 0.0446 with R^2 = 0.992 for $[\{Cu(L^2)\}_2(CN)](BF_4)_3$ ($\chi_{TIP} = 120 \times 10^{-6}$ cm^3 mol^{-1} for both systems; see Figure 2).

The X-band solid state EPR spectrum of powdered crystals of $[Cu(L^1)(CN)]BF_4$ at 35 K (see Figure 3a) is the one expected from spectroscopically characterized tetragonally distorted mononuclear Cu^{II} bispidine complexes.[51,52] Close examination of the perpendicular region reveals additional ligand hyperfine coupling. Numerical differentiation of the experimental spectrum in Figure 3a produces the second derivative spectrum (Figure 3b), which has significantly higher resolution in both the parallel and the perpendicular regions. Computer simulation (XSophe–Sophe-XeprView

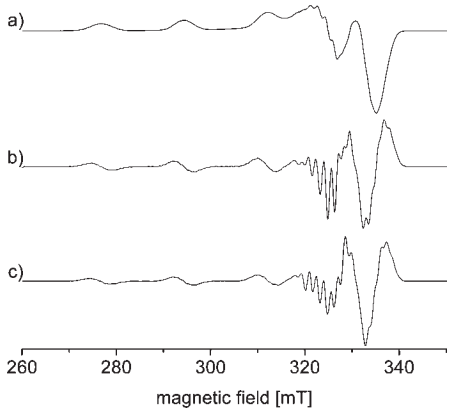

Figure 3. EPR-spectra of $[Cu(L^1)(CN)]BF_4$, (a) first derivative of the experimental spectrum measured at 35 K (ν = 9.352823 GHz), (b) second derivative of the experimental spectrum, (c) second derivative of the simulated spectrum.

computer simulation software suite[53]) of the first and second derivative EPR spectra (Figure 3 and Table 2) enabled the identification of nitrogen superhyperfine coupling not only from the pyridine nitrogens (py1, py2) and N3 but also from the CN ligand. The magnitude of A_N(CN) (Table 2) is consistent with carbon coordinated to the Cu^{II} ion as observed crystallographically (Figure 1). The solid state EPR spectrum of $[Cu(L^3)(CN)]BF_4$ (results not shown) revealed a single isotropic resonance around g~2, arising from intermolecular dipole–dipole interactions, and this was not characterized further.

Variable temperature X-band solid state EPR spectra were measured from powdered crystals of the homodinuclear Cu^{II} complexes $[\{Cu(L^n)\}_2(CN)](BF_4)_3$ (n = 1, 2), that is, of samples identical to those used for the SQUID measurements. The spectra were recorded in the temperature ranges of 6 to 78.5 K for $[\{Cu(L^1)\}_2(CN)](BF_4)_3$, and 5 to 72.5 K for $[\{Cu(L^2)\}_2(CN)](BF_4)_3$, respectively (see Supporting Information, Figures S1 and S2), and reveal the presence of multiple species. The spectra at the lowest temperatures (see Supporting Information, Figures S3a and S4a), where the triplet excited states are not populated, clearly show the presence of a large resonance attributable to a mononuclear Cu^{II} ($S = 1/2$) species, which is also present at higher temperatures (Supporting Information, Figures S1, S2). This is consistent with the magnetic susceptibility data described above. Since the Cu^{II} centers in the dinuclear species are antiferromagnetically

dx.doi.org/10.1021/ic102430a |Inorg. Chem. 2011, 50, 6890–6901

Table 2. Anisotropic Spin Hamiltonian Parameters for the Mononuclear Complex $[Cu(L^1)(CN)]BF_4$ and the Homodinuclear Cu^{II} Complexes $[\{Cu(L^1)\}_2(CN)](BF_4)_3$ and $[\{Cu(L^2)\}_2(CN)](BF_4)_3$ from Simulations of the EPR Spectra[a]

	$[Cu(L^1)\text{-}(CN)]BF_4$	$[\{Cu(L^1)\}_2\text{-}(CN)](BF_4)_3$	$[\{Cu(L^2)\}_2\text{-}(CN)](BF_4)_3$
		Cu^{II} Sites 1 and 2 Are Structurally and Electronically Identical[b]	
g_z	2.049	2.055	2.025
g_x	2.052	2.096	2.096
g_y	2.204	2.260	2.240
A_z [c]	18, 14, 8, 3[d]	8	8
A_x [c]	19, 12, 12, 4[d]	8	8
A_y [c]	179, 11, 13, 10[d]	195	190
		Interaction Hamiltonian Parameters[e]	
J		−104.3	−76.5
D_{exc}		−0.070	−0.159
E_{exc}/D_{exc}		0.205	0.080
G_x		−0.01176	
G_y		−0.00376	
G_z		0.0675	

[a] Crystallographic coordinates (site 1: $x = -9.1114$, $y = -0.1099$, $z = 7.68560$; site 2: $x = -8.99790$, $y = -5.11430$, $z = 8.37530$) for $[\{Cu(L^1)\}_2(CN)](BF_4)_3$ and (site 1: $x = 3.28980$, $y = -0.084800$, $z = 5.42030$; site 2: $x = -1.67180$, $y = -1.14730$, $z = 5.83000$) for $[\{Cu(L^2)\}_2(CN)](BF_4)_3$ were used to calculate the dipole−dipole interactions. [b] The g and A values for the second Cu site of $[\{Cu(L^1)\}_2(CN)](BF_4)_3$ are rotated into the coordinate system defined by Figure 1 using the Euler angles $\alpha = -6°$ and $\beta = 100°$. [c] In 10^{-4} cm^{-1}. [d] Hyperfine interaction with Cu, $N_{py1/py2}$, N3, N_{CN}; axis system defined as usual with the z-axis along the elongation (Cu−N7), that is, the labels are inverted with respect to the spectra of the homodinuclear systems ($z \rightarrow x$, $x \rightarrow y$, $y \rightarrow z$) [e] In cm^{-1}.

coupled (see magnetic data above), allowed and forbidden resonances from $\Delta M_S = \pm 1$ and ± 2 transitions within the excited triplet state ($S = 1$) only appear at higher temperatures (thermal population, Boltzmann distribution, Supporting Information, Figures S1, S2), and this depends on the singlet−triplet energy gap $-J$. At the best resolution of the triplet spectra (37.5 and 29 K for $[\{Cu(L^1)\}_2(CN)](BF_4)_3$ and $[\{Cu(L^2)\}_2(CN)](BF_4)_3$, respectively; see Supporting Information, Figures S3 and S4), we Fourier filtered the signal-averaged spectra to remove high frequency noise and then subtracted the EPR spectra of the mononuclear species at 6K to obtain the spectra of the dinuclear complexes shown in Figure 4 (see also Supporting Information). These spectra reveal the presence of allowed $\Delta M_s = \pm 1$ transitions around 200−450 mT and relatively intense and well resolved formally forbidden $\Delta M_s = \pm 2$ transitions around 150 mT. Computer simulation of the EPR spectra, also shown in Figure 4, employed a spin Hamiltonian ($\hat{H}_{Total}$, eq 2) consisting of the sum of the individual spin Hamiltonians ($\hat{H}_i$, $i = 1,2$) for the isolated Cu^{II} centers and the interaction Hamiltonian ($\hat{H}_{Int}$), which accounts for the isotropic (J), anisotropic ($\boldsymbol{D_{12}}$) and antisymmetric ($\boldsymbol{G_{12}}$) exchange interactions between the two Cu^{II} centers.[37,54,55]

$$\hat{H}_{Total} = \sum_{i=1}^{2} \hat{H}_i + \hat{H}_{Int} \quad (2.1)$$

$$\hat{H}_i = \beta \mathbf{s}_i \cdot \mathbf{g}_i \cdot \mathbf{B} + \mathbf{s}_i \cdot \mathbf{A}(Cu)_i \cdot \mathbf{I}(Cu)_i - g_n \beta_n \mathbf{B} \cdot \mathbf{I}(Cu)_i \quad (2.2)$$

$$\hat{\mathbf{H}}_{Int} = -J\mathbf{s}_1 \cdot \mathbf{s}_2 + \mathbf{s}_1 \cdot \mathbf{D}_{12} \cdot \mathbf{s}_2 + \mathbf{G}_{12} \cdot \mathbf{s}_1 \times \mathbf{s}_2 \quad (2.3)$$

In eq 2, $\mathbf{S}_i$ and $\mathbf{I}_i$ are the electron and nuclear spin vector operators, respectively, $\mathbf{g}_i$ and $\mathbf{A}_i$ are the electron Zeeman and hyperfine coupling matrices, respectively, g_n is the nuclear gyromagnetic ratio, β and β_n are the Bohr and nuclear magnetons, respectively, and $\boldsymbol{B}$ is the applied magnetic field. When the Cu···Cu internuclear distances are large, the anisotropic exchange contribution ($\boldsymbol{S_1 \cdot D_{12} \cdot S_2}$) to $\hat{H}_{Int}$ is negligible and, therefore, $\hat{H}_{Int}$ can be expressed by the dipole−dipole interaction between the Cu^{II} centers (see next section). However, when the positional coordinates from X-ray crystallography were incorporated into the Molecular Sophe (MoSophe) computer simulation suite,[56] the simulated ZFS arising from a purely dipole−dipole interaction was smaller than that observed experimentally. Consequently, we have modified MoSophe (v 2.1.6, see Experimental Section) to allow for additional anisotropic ZFS terms (added to the isotropic and dipole−dipole terms), which occur through a third order contribution from isotropic exchange to the anisotropic exchange interaction, that is proportional to $(\Delta g/g)^2$.[37] In our simulation of the EPR spectra of the two dinuclear complexes, we adopt the coordinate system (reference axes x, y, z, see Figure 1) in which the g-matrices of Cu1 and Cu2 are diagonal. We further assume that there are axial (D_{exc}) and orthorhombic (E_{exc}) ZFS contributions to the exchange tensor $\boldsymbol{D_{12}}$ and for $[\{Cu(L^1)\}_2(CN)](BF_4)_3$ an antisymmetric term (G_{12}).

MoSophe computer simulation of the experimental spectra for $[\{Cu(L^1)\}_2(CN)](BF_4)_3$ and $[\{Cu(L^2)\}_2(CN)](BF_4)_3$ (Figure 4a, processed as described in the Supporting Information), with the spin Hamiltonian given in eq 2, the parameters in Table 2, and the atomic coordinates of the two Cu^{II} centers, yield the spectra shown in Figure 4b. Not unexpectedly, it was also found necessary to include intermolecular dipole−dipole interactions between Cu^{II} ions in different molecules, as the closest $[\{Cu^{II}\}_2]\cdots[\{Cu^{II}\}_2]$ distance between two molecular units is only about 8 Å. To avoid an overparameterization, this perturbation was treated as purely isotropic with $g_{iso} = 2.137$, $A_{iso} = 70.3 \times 10^{-4}$ cm^{-1}, and an isotropic line width $\sigma B_{1/2} = 40 \times 10^{-4}$ cm^{-1} for $[\{Cu(L^1)\}_2(CN)](BF_4)_3$, and with $g_{iso} = 2.12$, $A_{iso} = 68.7 \times 10^{-4}$ cm^{-1}, and $\sigma B = 40 \times 10^{-4}$ cm^{-1} for $[\{Cu(L^2)\}_2(CN)](BF_4)_3$ ($g_{iso} = 1/3(g_x + g_y + g_z)$ and $A_{iso} = 1/3(A_x + A_y + A_z)$). While there is excellent agreement between the simulated (Figure 4c) and experimental spectrum (Figure 4a) for $[\{Cu(L^2)\}_2(CN)](BF_4)_3$ (B), the agreement between the simulated (Figure 4c) and experimental spectrum (Figure 4a) for $[\{Cu(L^1)\}_2(CN)](BF_4)_3$ (A) is not as good. This is a consequence of the lower symmetry of the complex and the resulting antisymmetric exchange (see ligand field analysis below). The spin Hamiltonian and structural parameters (internuclear Cu···Cu distance and orientation, Table 2) are in agreement with the observed structural data and the EPR parameters of the mononuclear complex. The g and A matrices are quite similar for $[\{Cu(L^1)\}_2(CN)](BF_4)_3$ and $[\{Cu(L^2)\}_2(CN)](BF_4)_3$ (see Table 2), but the axial ZFS parameters $\boldsymbol{D_{12}}$ (D_{exc}) and specifically the rhombicity E_{exc}/D_{exc} strongly differ for the two complexes. While inclusion of antisymmetric exchange (albeit smaller than predicted by ligand field theory) improved the quality of the simulation, the large number of parameters (3 g-, 3 A-, J, 2 D_{12}-, 3 G_{12}, their distributions (12) and 3 residual line width -parameters) precludes a unique solution without examination of the parameter surface in conjunction with measuring multifrequency EPR spectra.

The electronic absorption spectra consist of two transitions each with maxima at approximately 17,500 and 9,500 cm^{-1} for

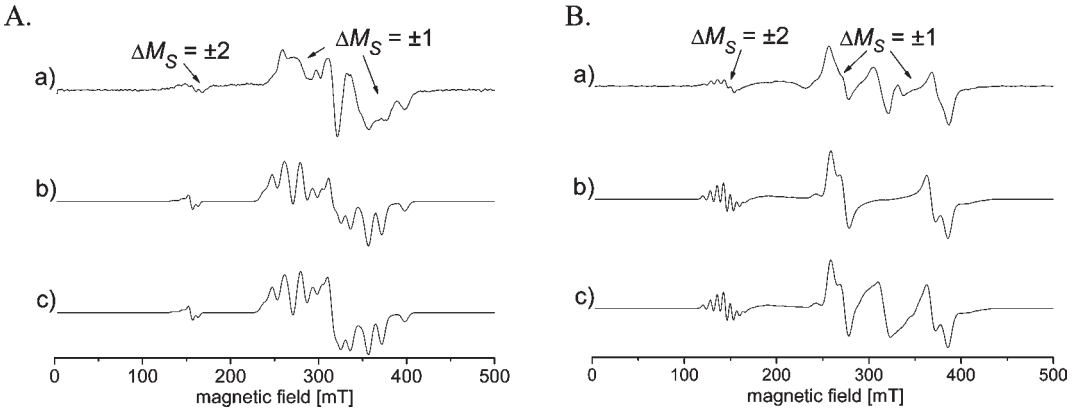

Figure 4. EPR-spectra of (A) $[\{Cu(L^1)\}_2(CN)](BF_4)_3 \cdot 1.35H_2O$ and (B) $[\{Cu(L^2)\}_2(CN)](BF_4)_3$. The arrows point to the resonances associated with the $\Delta M_S = \pm 1$ and ± 2 transitions of the dinuclear Cu complex. (a) Measured spectra at 37.5 K (ν = 9.40637 GHz) and 29 K (ν = 9.40372 GHz) for A and B, respectively. Resonances due to the Cu^{II} impurity have been subtracted from the experimental spectrum (see text and Supporting Information). (b) Simulated[56] spectra, taking only intramolecular interactions into account. (c) Simulation[56] with an additional isotropic intermolecular interaction, see text.

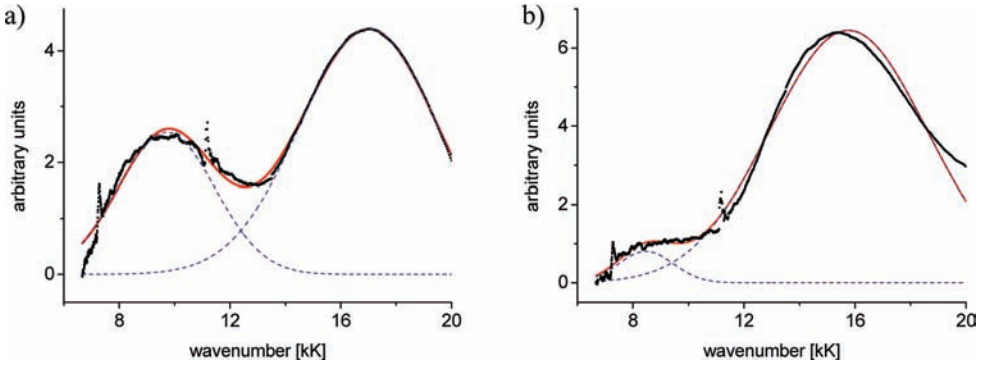

Figure 5. Ambient temperature diffuse reflectance absorption spectra of the d-d transitions of (a) $[\{Cu(L^1)\}_2(CN)](BF_4)_3 \cdot 1.35H_2O$ and (b) $[\{Cu(L^2)\}_2(CN)](BF_4)_3$, and their simulation with two Gaussian envelopes each ($F = b_3 \exp\{-[(x - b_1)/b_2]^2\} + b_6 \exp\{-[(x - b_4)/b_5]^2\}$); (a) b_1 = 9712 cm^{-1}, b_2 = 2476 cm^{-1}, b_3 = 2.539; b_4 = 17011 cm^{-1}, b_5 = 3531 cm^{-1}, b_6 = 4.391 and a standard deviation of 0.170; (b) b_1 = 8466 cm^{-1}, b_2 = 1394 cm^{-1}, b_3 = 0.804; b_4 = 15758 cm^{-1}, b_5 = 3994 cm^{-1}, b_6 = 6.453 and a standard deviation of 0.197.

$[\{Cu(L^1)\}_2(CN)]^{3+}$ (Figure 5a), and a maximum and a shoulder at 15,800 cm^{-1} and 8,500 cm^{-1} for $[\{Cu(L^2)\}_2(CN)]^{3+}$, respectively (Figure 5b). These are assigned to electronic transitions from e_g (d_{z^2}) and t_{2g} (d_{xy}, d_{xz}, d_{yz}) orbitals to the singly occupied $d_{x^2-y^2}$ orbital (e_g, all in O_h). The set of t_{2g} orbitals, which are diagonal in O_h, can split in low-symmetry ligand fields but, because of the weak π-overlap, these splittings are small (see Supporting Information, Table S1) and are, as usual for this type of Cu^{II} complexes, not resolved, leading to broad absorption bands with maxima at 17,500 and 15,800 cm^{-1} for the two complexes. A simulation of the d-d transitions with two Gaussian-type functions leads to transition energies of 9,712 and 17,011 cm^{-1} for $[\{Cu(L^1)\}_2(CN)]^{3+}$, and 8,466 and 15,758 cm^{-1} for $[\{Cu(L^2)\}_2(CN)]^{3+}$ (Figure 5).[57] There is a shift of over 1,000 cm^{-1} to higher energies of the d-d transitions of $[\{Cu(L^1)\}_2(CN)]^{3+}$ compared to those of $[\{Cu(L^2)\}_2(CN)]^{3+}$. The lower coordination number of the L^1-based complex (5 versus 6) leads to a lower symmetry and therefore to a larger splitting of the e_g- and t_{2g}-derived orbitals, and, because of larger off-centric distortions, also to an increased intensity of the 9,500 cm^{-1} band.

Theory and Data Analysis. *Isotropic Exchange Coupling Parameters J.* The exchange coupling parameters J of $[\{Cu(L^1)\}_2(CN)](BF_4)_3$ and $[\{Cu(L^2)\}_2(CN)](BF_4)_3$ were calculated with a well-established and validated broken-symmetry-based DFT approach,[58] using the B3LYP functional and a combination of TZVP and 6-31G* basis sets.[12] Single point DFT calculations for the *high-spin* and broken symmetry states were performed on the experimentally determined coordinates (Table 1), and the computation of the exchange coupling constants was based on a Heisenberg–Dirac–van Vleck spin Hamiltonian.[59] The computed exchange coupling constants J for $[\{Cu(L^1)\}_2(CN)](BF_4)_3$ (−64.3 cm^{-1}) and $[\{Cu(L^2)\}_2(CN)](BF_4)_3$ (−51.7 cm^{-1}) are in acceptable agreement with those emerging from the Bleaney–Bowers fit of the magnetic susceptibility data (see above).

Analysis of the Magnetic Anisotropy. A thorough ligand-field-theory-based analysis, which explicitly takes all micro states and all important interactions (Jahn–Teller and spin–orbit coupling) into account, is mandatory to thoroughly analyze the electronic interactions in exchange-coupled oligonuclear transition metal ion complexes.[18,19,38,39] Therefore, the experimentally determined magnetic susceptibilities and spectroscopic data (EPR, UV–vis–NIR) of $[\{Cu(L^1)\}_2(CN)](BF_4)_3$ and $[\{Cu(L^2)\}_2(CN)](BF_4)_3$ were analyzed with a ligand-field-theory-based approach.[6,7,60–62]

dx.doi.org/10.1021/ic102430a |*Inorg. Chem.* 2011, 50, 6890–6901

The energy levels of a pair of exchange coupled Cu^{II} ions are described by the Hamiltonian of eq 3,

$$\mathbf{H} = \mathbf{V}^1_{LF} + \mathbf{V}^2_{LF} + \zeta_1(\mathbf{s_1}\cdot\mathbf{l_1}) + \zeta_2(\mathbf{s_2}\cdot\mathbf{l_2}) + \mathbf{H}^{12}_{exch} + \mathbf{H}^1_Z + \mathbf{H}^2_Z \quad (3.1)$$

$$\mathbf{H}^{12}_{exch} = \sum_{\mu 1=1}^{5}\sum_{\nu 2=1}^{5} j_{\mu\nu}\mathbf{s}_{\mu 1}\cdot\mathbf{s}_{\nu 2} \quad (3.2)$$

where $\mathbf{V}^1_{LF}$ and $\mathbf{V}^2_{LF}$ are the operators of the ligand field of the Cu1 and Cu2 centers; $\zeta_1(\mathbf{s_1}\cdot\mathbf{l_1})$ and $\zeta_2(\mathbf{s_2}\cdot\mathbf{l_2})$ are the corresponding spin−orbit coupling operators (the effective spin−orbit coupling constants ζ_1 and ζ_2 for the two d^9 Cu^{II} ions are defined as negative, see Supporting Information, Table S1); $\mathbf{H}^1_Z$ and $\mathbf{H}^2_Z$ are the Zeeman operators, that is, $\mu_B(2\boldsymbol{s_1} + k_1\mathbf{l_1})$ and $\mu_B(2\boldsymbol{s_2} + k_2\mathbf{l_2})$ with the spin angular momentum operator $\boldsymbol{s_i}$ ($\boldsymbol{s_{ix}}$, $\boldsymbol{s_{iy}}$, $\boldsymbol{s_{iz}}$, $i = 1,2$) and the orbital angular momentum operator $\boldsymbol{l_i}$ ($\boldsymbol{l_{ix}}$, $\boldsymbol{l_{iy}}$, $\boldsymbol{l_{iz}}$, $i = 1, 2$), acting on each Cu^{II} site, and with the usual covalent reduction factor k_i ($i = 1, 2$); $\mathbf{H}^{12}_{exch}$ is the exchange coupling operator, which describes the exchange interaction between Cu1 and Cu2; the Heisenberg exchange integrals $j_{\mu\nu}$ describe the effective coupling of two spins in the magnetic orbitals $\mu 1$ of Cu1 and $\nu 2$ of Cu2. In the following, we approximate the matrix $j_{\mu\nu}$ with two parameters (the exchange coupling energy j_σ between the unpaired spins of each Cu^{II}, residing in d_{z^2} orbitals parallel to the Cu···Cu vector, and the exchange coupling energy $j_{\sigma\pi}$ between the spins on d_{z^2}(Cu1) and $d_{xz,yz}$(Cu2) or vice versa).

The Hamiltonian of eq 3 operates within the basis of the 100 micro states of the pair of Cu^{II} ions, which result from the combination of each of the 10 spin orbitals of Cu1 with those of Cu2. The dicopper(II) complexes discussed here are significantly distorted (Figure 1 and Table 1), and this leads to an orbitally nondegenerate ground state for each Cu^{II} site. The Hamiltonian of eq 3, combined with experimental data from optical and EPR spectra and magnetic measurements, was used to derive the spin Hamiltonian parameters and compare them with those obtained by simulation of the EPR spectra.

Ligand Fields and g-Tensor Values. The angular overlap model (AOM), with a $1/r^6$ dependence of the e_σ and e_π parameters (r is the metal−ligand distance)[63,64] and the energies of the d-d transitions from the observed absorption bands, was used to deduce the matrices of the ligand field at the Cu1 and Cu2 sites, geometrically defined by the X-ray structural data. From these matrices, combined with spin−orbit coupling, the ground state g-tensor values were deduced following a well-documented procedure.[65] This tensor $\boldsymbol{g}$ is real, off-diagonal and nonsymmetric, and is brought to a diagonal form by diagonalization of $\boldsymbol{g}^T\cdot\boldsymbol{g}$, where $\boldsymbol{g}^T$ is the transpose of $\boldsymbol{g}$, and the eigenvectors yield the direction in which $\boldsymbol{g}$ becomes diagonal. The corresponding axes were chosen to reorient the molecule (see Figure 1), and were used for the analysis of the spin-Hamiltonian and the magnetic parameters: the z-axis is parallel to the Cu···Cu vector, and the x- and y-axes, are nearly perpendicular and parallel to the long (Jahn−Teller) axis, respectively (the ligand field matrices for this choice of axes are listed in the Supporting Information, Table S1).

ZFS Tensor. The ZFS tensor $\boldsymbol{D_{12}}$ for a pair of coupled $S = 1/2$ ions consists of dipolar and exchange parts (eq 3.3). The dipolar part is approximated on the basis of the expression for two interacting dipoles and the known geometry (see the Supporting Information, eqs S8−S10).[66]

$$\mathbf{D}_{12} = \mathbf{D}_{exc} + \mathbf{D}_{dip} \quad (3.3)$$

In the approximation that the tensors g, $\boldsymbol{D}_{exc}$, and $\boldsymbol{G}_{exc}$ can be reduced to a diagonal form *simultaneously*, the ZFS tensor is simplified to its conventional form given by

$$\begin{aligned}\hat{\mathbf{H}}^D_{exc} &= D_{xx}\mathbf{s_{1x}}\cdot\mathbf{s_{2x}} + D_{yy}\mathbf{s_{1y}}\cdot\mathbf{s_{2y}} + D_{zz}\mathbf{s_{1z}}\cdot\mathbf{s_{2z}}\\ &= \frac{2}{3}D_{exc}(2\mathbf{s_{1z}}\cdot\mathbf{s_{2z}} - \mathbf{s_{1x}}\cdot\mathbf{s_{2x}} - \mathbf{s_{1y}}\cdot\mathbf{s_{2y}})\\ &\quad + E_{exc}(\mathbf{s_{1x}}\cdot\mathbf{s_{2x}} - \mathbf{s_{1y}}\cdot\mathbf{s_{2y}})\end{aligned} \quad (3.4)$$

with D_{xx}, D_{yy}, and D_{zz} expressed in terms of the axial D_{exc} and orthorhombic E_{exc} parameters given by eq 3.5. D_{exc} and E_{exc} were calculated from the three lowest eigenvalues $E_1 < E_2 < E_3$ of eq 3.1 (without the Zeeman terms eq 3.6).

$$\begin{aligned}D_{xx} &= E_{exc} - \frac{2}{3}D_{exc}\\ D_{yy} &= -E_{exc} - \frac{2}{3}D_{exc}\\ D_{zz} &= \frac{4}{3}D_{exc}\end{aligned} \quad (3.5)$$

$$\begin{aligned}D_{exc} &= E_1 - (E_2 + E_3)/2\\ E_{exc} &= (E_2 - E_3)/2\end{aligned} \quad (3.6)$$

The exchange parameters j_σ and $j_{\sigma\pi}$ were adjusted to reproduce the values of J, deduced from a fit of the magnetic susceptibility data (eq 1, Figure 2), and values of D_{exc} and E_{exc}, obtained from simulation of the EPR spectra (Table 2, Figure 4). A list of all model parameters is given in Table 3. To account for the off-diagonal elements of the symmetric $\boldsymbol{D}_{exc}$ and antisymmetric $\boldsymbol{G}_{exc}$ tensors, the terms of eq 3.7 are introduced in eq 3.4, and the six D_{ij} and three G_i parameters are determined.

$$\begin{aligned}&D_{xy}(\mathbf{s_{1x}}\cdot\mathbf{s_{2y}} + \mathbf{s_{1y}}\cdot\mathbf{s_{2x}}) + D_{xz}(\mathbf{s_{1x}}\cdot\mathbf{s_{2z}} + \mathbf{s_{1z}}\cdot\mathbf{s_{2z}})\\ &+ D_{yz}(\mathbf{s_{1y}}\cdot\mathbf{s_{2z}} + \mathbf{s_{1z}}\cdot\mathbf{s_{2y}}) + G_x(\mathbf{s_{1y}}\cdot\mathbf{s_{2z}} - \mathbf{s_{1z}}\cdot\mathbf{s_{2y}})\\ &+ G_y(\mathbf{s_{1z}}\cdot\mathbf{s_{2x}} - \mathbf{s_{1x}}\cdot\mathbf{s_{2z}}) + G_z(\mathbf{s_{1x}}\cdot\mathbf{s_{2y}} - \mathbf{s_{1y}}\cdot\mathbf{s_{2x}})\end{aligned} \quad (3.7)$$

With the known set of parameters (Table 2) the matrix of eq 3.1 (without the Zeeman terms) is diagonalized in two steps. In the first step the matrix of the ligand field and exchange coupling (eq 3.2) is diagonalized without spin−orbit coupling to yield pure spin triplet and singlet eigenvectors. Then, the spin−orbit coupling matrix $\zeta_1(\mathbf{s_1}\cdot\mathbf{l_1}) + \zeta_2(\mathbf{s_2}\cdot\mathbf{l_2})$ is transformed into this basis. The lowest four eigenvalues and eigenfunctions of this matrix account for the effect of spin−orbit coupling on the ground state singlet and triplet states. The diagonal matrix with the eigenvalues ε_i, i = 1,4 and the corresponding truncated eigenvectors C(1:4, i) are denoted Λ and $\boldsymbol{U}$, respectively. The matrix $\boldsymbol{U}$ is neither orthogonal nor normalized; however, by a procedure described previously, it can be brought to such a form $\boldsymbol{C}$.[67] With Λ and $\boldsymbol{C}$, we calculate the ZFS matrix $\mathbf{H}^{LF}_{ZFS}$, derived from eqs 3.1 and 3.2:

$$\mathbf{H}^{LF}_{ZFS} = \mathbf{C}\cdot\Lambda\cdot\mathbf{C}^\dagger \quad (3.8)$$

dx.doi.org/10.1021/ic102430a |*Inorg. Chem.* 2011, 50, 6890–6901

Table 3. Calculated *g*-Tensor Parameters, with the Corresponding Spin-Orbit Coupling (ζ), Obital Reduction (k), and Exchange Parameters (j_σ, $j_{\sigma\pi}$), and the Cu···Cu Distances (From the Experimental Structures, Table *1*), Adopted for the Calculation of the ZFS Parameters, Given in Table *4*

	$[\{Cu(L^1)\}_2CN)]^{3+}$ [a]	$[\{Cu(L^2)\}_2CN)]^{3+}$ [a]
g_{1x}	2.073	2.066
g_{1y}	2.265	2.290
g_{1z}	2.041	2.052
g_{2x}	2.265	2.066
g_{2y}	2.073	2.290
g_{2z}	2.041	2.052
ζ	622	622
k	0.866	0.866
j_σ	−169.8	−128.1
$j_{\sigma\pi}$	46.9	78.0
$R_{Cu1\cdots Cu2}$	5.053	5.091

[a] Calculated by the ligand field matrix elements from the Supporting Information, Table S1; ζ and k are given in the table, and the coordinate system is defined in Figure 1.

Table 4. Exchange Contributions to the Parameters of the Spin Hamiltonian (in cm^{-1}) for the $[\{Cu(L^1)\}_2CN)]^{3+}$ and $[\{Cu(L^2)\}_2CN)]^{3+}$ Dinuclear Complexes[a]

	$[\{Cu(L^1)\}_2CN)]^{3+}$	$[\{Cu(L^2)\}_2CN)]^{3+}$
J	−104.3	−76.5
D_{xx}	0.135	0.109
D_{yy}	0.022	0.062
D_{zz}	−0.158	−0.171
D_{xy}	0.028	0.002
D_{xz}	−0.037	−0.007
D_{yz}	−0.003	−0.109
G_x	−6.032	0
G_y	−0.797	0
G_z	1.016	0

[a] Calculations were done with model parameters from Table 3 and Supporting Information, Table S1.

Note that the matrices $\mathbf{H}^{LF}_{ZFS}$(eq 3.8) and $\hat{\mathbf{H}}^{D}_{exc}$ (eqs 3.4, 3.7) are represented with different basis functions: the spin-coupled singlet ($S = 0$) and triplet ($S = 1$, $M_s = -1,0,1$) in $\mathbf{H}^{LF}_{ZFS}$, and, in $\hat{\mathbf{H}}^{D}_{exc}$, spin-uncoupled product functions $\alpha_1\alpha_2$, $\beta_1\alpha_2$, $\alpha_1\beta_2$, and $\beta_1\beta_2$ for the $S = 1/2$ spins on centers Cu1 and Cu2. However, a transformation of $\hat{\mathbf{H}}^{D}_{exc}$ from the latter to the former basis $\hat{\mathbf{H}}^{D'}_{exc}$ is possible (see Supporting Information, eq S5). The comparison of $\mathbf{H}^{LF}_{ZFS}$ with $\hat{\mathbf{H}}^{D'}_{exc}$ yields the values for the parameters D_{ij} and G_i listed in Table 4 and explicitily derived in the Supporting Information, eqs S7.1−S7.10.

$[\{Cu(L^2)\}_2(CN)]^{3+}$. The ground state of the Cu^{II} centers is $d_{z^2-x^2} = (\sqrt{3}/2)d_{z^2} - (1/2)d_{x^2-y^2}$, and the computed local *g*-matrix values have one large ($g_{1y} = g_{2y} = 2.29$) and two small components ($g_{1z} = g_{2z} = 2.052$, $g_{1x} = g_{2x} = 2.066$), that is, the calculated *g*-matrix is typical for tetragonally elongated hexacoordinate Cu^{II} complexes with a small but significant orthorhombic splitting. These values are in reasonable agreement with those derived from the simulation of the EPR spectrum (Table 2). In agreement with the simulations, the results show important contributions from both dipolar and exchange coupling with a clear dominance of the latter. With the disorder of the CN^- bridging ligand and the resulting effective center of inversion in our treatment, the parameters of the antisymmetric exchange ($\mathbf{G}_{exc}$, eq 2.3, Table 4) are zero. It is remarkable that, because of the orthogonality between the singly occupied $d_{z^2-x^2} = (\sqrt{3}/2)d_{z^2} - (1/2)d_{x^2-y^2}$ orbital of Cu1 and the doubly occupied d_{xz} and d_{yz} orbitals of Cu2 (or vice versa) the value of $j_{\sigma\pi}$ is positive (Table 3), that is, it leads to ferromagnetic coupling between the spin of Cu1 in its ground state with the spin of Cu2 in its π-excited state (or vice versa). A positive value has also been calculated by DFT for a Cu^{II}-NC-Fe^{III} pair ($j_{\sigma\pi} = 20\ cm^{-1}$).[6] The positive $j_{\sigma\pi}$ leads to the calculated negative sign of *D*. A qualitatively similar result, based on high-field, high-frequency EPR measurements was recently reported for the classical copper(II) acetate monohydrate complex,[3] for which a reversed sign has been reported in the classical paper by Bleaney and Bowers.[2] It is interesting to deduce by diagonalization of the symmetric tensor D_{exc} that the ease axis of magnetization of the excited spin triplet state makes the smallest angle (21.6°) with the Cu···Cu vector (*z* axis), and it is approximately perpendicular to the pseudo-Jahn−Teller axes (*y* axes), which also yields the largest value of *g* (see Figure 1, Tables 1, 2).

$[\{Cu(L^1)\}_2(CN)]^{3+}$. As in the previous section on $[\{Cu(L^2)\}_2(CN)]^{3+}$, the coordination geometry of Cu1 is such that the *y*- and *x*-axes are nearly parallel and perpendicular to the long bond, respectively, but for Cu2 the two axes are interchanged (the two Cu^{II} sites are rotated with respect to each other around the *z*-axis by approximately 90°, see Figure 1). Therefore, the ground states of Cu1 and Cu2 differ: for Cu1 it is $d_{z^2-x^2} = (\sqrt{3}/2)d_{z^2} - (1/2)d_{x^2-y^2}$ and for Cu2 it is $d_{z^2-y^2} = (\sqrt{3}/2)d_{z^2} + (1/2)d_{x^2-y^2}$. With one large $g_{1y} = g_{2x} = 2.265$ and two small $g_{1x} = g_{2y} = 2.073$, $g_{1z} = g_{2z} = 2.041$ components (Table 3), the *g*-matrix is typical for tetragonal hexacoordinate complexes of Cu^{II}, largely axial but with a significant orthorhombic splitting, and this is in agreement with the values deduced from the experimental spectrum (see Tables 2). As for complex $[\{Cu(L^2)\}_2(CN)]^{3+}$, the ease axis of magnetization of the excited spin triplet state nearly coincides with the Cu···Cu vector (here with an angle of only 7.1° to the *z*-axis). That is, the ease axis is again approximately perpendicular to the pseudo-Jahn−Teller axes of the Cu^{II} centers but here, these are rotated toward each other, that is, for Cu1 it is the *y*- and for Cu2 the *x*-axis with a maximum *g*-tensor parameter.

The rather large value of the antisymmetric exchange tensor parameter G_x (see Table 4), related to the lack of a center of inversion, leads to a pronounced mixing between the $S = 0$ ground and $S = 1$ excited spin states (see Supporting Information, eq. S5). Antisymmetric exchange G_i and off-diagonal D_{ij} parameters have been considered in the simulation of the EPR spectrum (Figure 4 and Table 2; see Supporting Information for more details). However, as noted above, because of the large number of parameters and the fact that the EPR spectra are mixtures with some mononuclear impurity, these simulations should not be overinterpreted.

CONCLUSIONS

The Cu^{II} complexes of the bispidines L^1, L^2, and L^3 have, in terms of the pseudo-Jahn−Teller axes strikingly different geometries, and with L^1 and L^2, where the monodentate coligand has a strong in-plane bond, stable homodinuclear complexes were obtained. In contrast, with L^3, where the CN^- coligand is on the pseudo-Jahn−Teller axis, no homodinuclear complexes were

dx.doi.org/10.1021/ic102430a |*Inorg. Chem.* 2011, 50, 6890–6901

isolated because of the weak bond to the bridging ligand. While the L^1-based system has five-coordinate Cu^{II} centers, those of the L^2-based dimer are six-coordinate. Because of the differing steric demand of the two ligand systems, there are important structural differences of the two dicopper(II) complexes, primarily with respect to the relative orientation of the two local coordinate systems. This leads to subtle differences in the electronic and magnetic properties, in particular with respect to the rhombicity of the ZFS and the resulting antisymmetric exchange in $[\{Cu(L^1)\}_2(CN)]^{3+}$.

With a ligand-field-theory-based model and exploiting as much as possible magnetic, EPR, and optical spectroscopy to deduce its parameters, a deep understanding of the origin of the magnetic anisotropy of the excited spin-triplet state was achieved. A very large and positive exchange coupling between the σ-type ground state of one Cu^{II} center and the $\pi(d_{xz},d_{yz})$ excited state of the neighboring Cu^{II} center (and vice versa) is found to be responsible for the negative ZFS of the excited spin-triplet state of the Cu_2 pair. In the case of $[\{Cu(L^1)\}_2(CN)]^{3+}$ antisymmetric exchange contributes to the EPR resonances, and, with a single data set, this is difficult to accurately simulate because of the number of spin Hamiltonian and line width parameters involved.

EXPERIMENTAL SECTION

Measurements. *Infrared spectra* (KBr pellets) were recorded with a Spectrum 100 FT-IR-Spectrometer (Perkin-Elmer).

EPR (Powder X-band, 9.5 GHz) spectra were recorded on a Bruker Biospin Elexsys E500 spectrometer with a rectangular TE_{102} cavity mode. The system is equipped with an Oxford Instruments ESR 900 continuous liquid helium flow cryostat in conjunction with an ITC 4 temperature controller. The microwave frequency and magnetic field were calibrated with a Hewlett-Packard frequency counter and DPPH ($g = 2.0036$) as a field marker. The EPR spectra (Figure 4a) were Fourier filtered to remove the high frequency noise (Hamming function), and the EPR signal attributable to the mononuclear species was subtracted. Computer simulations were performed with the Molecular Sophe computer simulation software suite (v2.1.6) running on a Linux platform with either Mandriva 2010 or openSuSE 11.1 as an operating system.[56] Version 2.1.6 of Molecular Sophe now has seven exchange representations, including isotropic, anisotropic-axial, anisotropic-axial diagonal, anisotropic-orthorhombic, anisotropic-orthorhombic diagonal, antisymmetric, general, general-diagonal. The diagonal and general representations are new. The general-diagonal exchange representation utilizes the Hamiltonian given in eq 2 and the parameters, J_{iso}, J_D, $J_{E/D}$, α, β, γ and V_x, V_y, V_z, V_α, V_β, V_γ; where $J_D = D_{exc}$; $J_{E/D} = E_{exc}/D_{exc}$ and $V = G$ in eq 2. The computational program, Sophe, a component of the Molecular Sophe computer simulation software suite[56] employs matrix diagonalization, and consequently for the general-diagonal representation we employed all three exchange terms given in eq 2 in conjunction with eq 1 for both Cu(II) centers to create the energy matrix for the dinuclear Cu(II) center.

Magnetic measurements were carried out on a MPMS-XL 5T (Quantum Design) SQUID-Magnetometer. Samples were powdered and pressed in PTFE tape to avoid field-induced orientation. The data were corrected for diamagnetism of the sample holder, and Pascal's constants were used for diamagnetic corrections of the sample.[68]

Elemental analyses were obtained from the microanalytical laboratory of the Chemical Institutes of the University of Heidelberg.

X-ray Crystal Structure Determinations. *Crystal data* and details of the structure determinations are listed in Table 5. Intensity data were collected at low temperature with a STOE IPDS1 image plate ($[Cu(L^1)(CN)]BF_4$) and a Bruker AXS Smart 1000 CCD diffractometer (all others) (Mo−K_α radiation, graphite monochromator, $\lambda = 0.71073$ Å). Data from the Smart 1000 were corrected for air and detector absorption, Lorentz and polarization effects.[69] Absorption by the crystal was treated with a semiempirical multiscan method.[70,71] Absorption correction of the data from the IPDS was done numerically.

The structures were solved by conventional direct methods[72,73] ($[\{Cu(L^1)\}_2(CN)](BF_4)_3\cdot 1.35H_2O$ and $[Cu(L^1)(CN)]BF_4$) or by the heavy atom method combined with structure expansion by direct methods applied to difference structure factors[74,75] (all others), and refined by full-matrix least-squares methods based on F^2 against all unique reflections.[73,76] All non-hydrogen atoms were given anisotropic displacement parameters. In the mononuclear complexes both possible coordination modes of the cyanide ligand (C- or N-bound) were considered, with refinement indicating strong preference for the C-bound coordination mode in both complexes. Most hydrogen atoms (except those of the located solvent water molecules, where suitable positions could not be geometrically derived) were input at calculated positions and refined with a riding model. Appropriate distance and bond angle constraints were applied to the $[BF_4]^-$ anions. In the structure of $[\{Cu(L^2)\}_2(CN)](BF_4)_3$ the occupancy of the $[BF_4]^-$ anions was constrained to add up to 1.5 (3 $[BF_4]^-$ per complex cation). Invariably, the dimetallic complexes had a crystallographic center of symmetry, which resulted in a 1:1 disorder of the bridging cyanide ligand. The structures frequently contained disordered and/or partially occupied solvent molecules (water, methanol, nitromethane). Whenever possible, these were included in the refined model. In some cases (complexes $[Cu(L^1)(CN)]BF_4$, $[\{Cu(L^1)\}_2(CN)](BF_4)_3\cdot 1.35H_2O$, $[\{Cu(L^2)\}_2(CN)](BF_4)_3$, and $[\{Ni(L^3)\}_2(CN)](BF_4)_3$) all or parts of the electron density attributed to solvent of crystallization was removed from the structures (and the corresponding F_{obs}) with the BYPASS procedure,[77] as implemented in PLATON (SQUEEZE).[78,79] CIF files giving crystallographic data for compounds $[Cu(L^1)(CN)]BF_4$, $[Cu(L^3)(CN)]BF_4$, $[\{Cu(L^1)\}_2(CN)](BF_4)_3\cdot 1.35H_2O$, $[\{Cu(L^2)\}_2(CN)](BF_4)_3$, and $[\{Ni(L^3)\}_2(CN)](BF_4)_3$ are available as Supporting Information.

Computational Procedures. The exchange coupling constants were calculated with the program package ORCA versions 2.6.04 and 2.6.35,[80] using the hybrid density functional B3LYP.[81−83] Either a mixed basis set approach, that is, the TZVP basis[84,85] for the metal centers and the atoms of the first coordination sphere and the 6-31G* basis set[86−95] for the remaining atoms, or the singly polarized double-ζ quality basis def-SV(P))[84] were used. Single point calculations for the *high-spin* and broken symmetry state were performed on the geometries defined by the X-ray structures and converged to an energy threshold of 10^{-7} hartree.

Angular overlap model calculations of the d-d spectra of the two dicopper(II) complexes and their ligand field matrices (Supporting Information, Table S1) were performed with the AOMX program package;[96] spin multiplet, spin-Hamiltonian parameters, and magnetic susceptibilities were calculated with programs written in MatLab.[97]

Syntheses. *General Procedures and Ligands.* Chemicals were used as supplied. Technical grade solvents were distilled prior to use. The ligands L^1, L^2, and L^3 were prepared as described previously.[26,98,99]

Caution! *Cyanide salts are very toxic and should be handled in a well ventilated fume hood*

Bispidine Complexes. The copper(II) complexes of L^1, L^2, and L^3 were synthesized according to published methods[51,100,101] with copper(II) tetrafluoroborate hydrate as copper(II) salt. As well as the copper(II) complexes, $[Ni(L^3)](BF_4)_2$ was synthesized according to published methods, using nickel(II) tetrafluoroborate hydrate as nickel(II) salt.

$[Cu(L^1)(CN)]BF_4$. To $[Cu(L^1)](BF_4)_2\cdot 2H_2O$ (730 mg, 1 mmol) in nitromethane (10 mL) was added a solution of tetraethylammonium-cyanide (156 mg, 1 mmol) in nitromethane (5 mL). The solution was stirred at room temperature for a short time, and the solvent removed by rotary evaporation. The resulting crude product was suspended in a small amount of MeOH, filtered and washed again with MeOH. Single crystals

Table 5. Crystal Data and Structure Refinement for the Complexes $[\{Cu(L^1)\}_2(CN)](BF_4)_3 \cdot 1.35H_2O$, $[\{Cu(L^2)\}_2(CN)](BF_4)_3$, $[Cu(L^1)(CN)]BF_4$, $[Cu(L^3)(CN)]BF_4$, and $[\{Ni(L^3)\}_2(CN)](BF_4)_3$

	$[\{Cu(L^1)\}_2(CN)](BF_4)_3 \cdot 1.35H_2O$	$[\{Cu(L^2)\}_2(CN)](BF_4)_3$	$[Cu(L^1)(CN)]BF_4$	$[Cu(L^3)(CN)]BF_4$	$[\{Ni(L^3)\}_2(CN)](BF_4)_3$
empirical formula	$C_{47}\ H_{58.70}\ B_3\ Cu_2\ F_{12}\ N_9\ O_{13.35}$	$C_{57}\ H_{62}\ B_3\ Cu_2\ F_{12}\ N_{11}\ O_{12}$	$C_{24}\ H_{28}\ Cu\ F_4\ N_5\ O_6$	$C_{30}\ H_{33}\ B\ Cu\ F_4\ N_6\ O_6$	$C_{59}\ H_{66}\ B_3\ F_{12}\ N_{11}\ Ni_2\ O_{12}$
formula weight	1350.84	1480.69	632.86	723.97	1499.08
temperature/K	100(2)	100(2)	200(2)	100(2)	100(2)
crystal system	monoclinic	triclinic	triclinic	monoclinic	orthorhombic
space group	$C2/c$	$P\bar{1}$	$P\bar{1}$	$P2_1/n$	$Ccc2$
unit cell dimensions a/Å	10.927(1)	10.7803(12)	9.182(2)	15.0345(16)	11.079(6)
b/Å	32.212(4)	11.4326(13)	11.544(2)	9.9685(11)	34.385(18)
c/Å	17.670(2)	15.2066(17)	14.416(3)	20.304(2)	35.122(18)
α/deg	90	78.649(2)	93.71(3)	90	90
β/deg	91.066(2)	70.449(2)	95.65(3)	98.743(2)	90
γ/deg	90	71.260(2)	109.51(3)	90	90
volume/Å	6218(1)	1664.1(3)	1425.6(5)	3007.6(6)	13379(13)
Z	4	1	2	4	8
density (calc.)/ $Mg \cdot m^{-3}$	1.443	1.478	1.474	1.599	1.488
absorption coefficient/mm^{-1}	0.784	0.739	0.839	0.807	0.664
F_{000}	2766	758	650	1492	6176
crystal size/mm^3	0.11 × 0.09 × 0.06	0.10 × 0.07 × 0.04	0.74 × 0.48 × 0.19	0.20 × 0.20 × 0.15	0.26 × 0.16 × 0.11
θ range for data collection/deg	2.0 to 25.2	1.9 to 26.4	1.9 to 25.0	1.8 to 32.3	1.2 to 26.4
index range h, k, l (indep. set)	−13 to 13, 0 to 38, 0 to 21	−12 to 13, −13 to 14, 0 to 18	−10 to 10, −13 to 13, 0 to 16	−21 to 21, 0 to 14, 0 to 30	0 to 13, 0 to 42, −43 to 43
reflections collected	51029	30953	10291	75769	124490
independent reflections [R_{int}]	5548 [0.0742]	6804 [0.0625]	4752 [0.0589]	10173 [0.0343]	13689 [0.0723]
observed reflections [$I > 2\sigma(I)$]	3834	5034	3205	8416	10835
max., min transmission	0.7452, 0.6455	0.7456, 0.6901	0.8566, 0.6674	0.7464, 0.6899	0.7464, 0.6725
data/restraints/parameters	5548/81/400	6804/59/467	4752/21/370	10173/21/438	13689/51/904
goodness-of-fit on F^2	1.169	1.091	0.876	1.091	1.058
R indices [$F_o > 4\sigma(F_o)$] $R(F)$, $wR(F^2)$	0.0670, 0.1929	0.0571, 0.1625	0.0420, 0.0935	0.0455, 0.1219	0.0458, 0.1105
R indices (all data) $R(F)$, $wR(F^2)$	0.1026, 0.2109	0.0833, 0.1778	0.0657, 0.0978	0.0599, 0.1345	0.0723, 0.1239
largest diff. peak and hole/$e \cdot Å^{-3}$	0.103, 1.488, −0.754	0.119, 1.447, −0.766	0.076, 0.398, −0.534	0.104, 1.183, −0.620	0.081, 0.789, −0.578

dx.doi.org/10.1021/ic102430a |*Inorg. Chem.* 2011, 50, 6890–6901

were obtained after a few days by slow evaporation of the mother liquor. The blue-violet product was vacuum-dried. Yield: 132 mg (21%). Anal. (%) Calcd for $[Cu(L^1)(CN)]BF_4$: C, 45.55; H, 4.46; N, 11.07. Found: C, 45.44; H, 4.41; N, 11.27. IR $\nu(C{\equiv}N)/cm^{-1}$: 2152 (m), 2125 (b).

$[Cu(L^3)(CN)]BF_4$. To $[Cu(L^3)](BF_4)_2 \cdot H_2O$ (789 mg, 1 mmol) in nitromethane (5 mL) was added a solution of tetraethylammonium-cyanide (188 mg, 1.2 mmol) in nitromethane (5 mL). The solution was stirred for 2 days at room temperature, and the solvent removed by rotary evaporation. The resulting crude product was suspended in a small amount of MeOH, filtered and washed again. Single crystals were obtained after a few days by slow evaporation of the mother liquor. The blue product was vacuum-dried. Yield: 452 mg (62%). Anal. (%) Calcd for $[Cu(L^3)(CN)]BF_4$: C, 49.77; H, 4.59; N, 11.61. Found: C, 49.31; H, 4.75; N, 11.59. IR $\nu(C{\equiv}N)/cm^{-1}$: 2140 (m).

$[\{Cu(L^1)\}_2(CN)](BF_4)_3 \cdot 1.35H_2O$. To $[Cu(L^1)](BF_4)_2 \cdot 2H_2O$ (371 mg, 0.51 mmol) in hot methanol (20 mL) was added a hot solution of $[Cu(L^1)(CN)]BF_4$ (316 mg, 0.5 mmol) in nitromethane (10 mL). The solution was stirred for a short time, and after cooling, the solvent was removed by rotary evaporation. The resulting crude product was suspended in a small amount of MeOH, filtered and washed again. Single crystals were obtained after a few days by slow evaporation of the mother liquor. The blue-violet product was vacuum-dried. Yield: 123 mg (18%). Anal. (%) Calcd for $[\{Cu(L^1)\}_2(CN)](BF_4)_3 \cdot 2MeOH$: C, 42.32; H, 4.64; N, 9.07. Found: C, 42.49; H, 4.88; N, 8.97. IR $\nu(C{\equiv}N)/cm^{-1}$: 2182 (b).

$[\{Cu(L^2)\}_2(CN)](BF_4)_3$. To $[Cu(L^2)](BF_4)_2 \cdot H_2O$ (394 mg, 0.5 mmol) in nitromethane (10 mL) was added NaCN (40 mg, 0.82 mmol) in H_2O (10 mL). The solution was stirred at room temperature for 2 days, and the solvent removed by rotary evaporation. The resulting crude product was suspended in a small amount of MeOH, filtered, and washed again. Single crystals were obtained after a few days by slow evaporation of the mother liquor. The blue product was vacuum-dried. Yield 82 mg (27%). Anal. (%) Calcd for $[\{Cu(L^2)\}_2(CN)](BF_4)_3$: C, 46.24; H, 4.22; N, 10.41. Found: C, 46.21; H, 4.25; N, 10.44. IR $\nu(C{\equiv}N)/cm^{-1}$: 2165 (b).

$[\{Ni(L^3)\}_2(CN)](BF_4)_3 \cdot 2H_2O$. To $[Ni(L^3)](BF_4)_2 \cdot 2H_2O$ (401 mg, 0.5 mmol) in methanol (10 mL) was added tetrabutylammonium cyanide (67 mg, 0.25 mmol) in methanol (5 mL). The solution was stirred at room temperature for a short period. Single crystals were obtained after 1 day by slow evaporation of the solvent. The pink product was vacuum-dried. Yield 185 mg (48%). Anal. (%) Calcd for $[\{Ni(L^3)\}_2(CN)](BF_4)_3 \cdot 2H_2O$: C, 46.16; H, 4.60; N, 10.04. Found: C, 45.99; H, 4.54; N, 10.09. IR $\nu(C{\equiv}N)/cm^{-1}$: 2150 (b).

■ ASSOCIATED CONTENT

Supporting Information. Details on the ligand field calculations with the corresponding parameter values and matrix elements, temperature-dependent susceptibilities and EPR spectra, powder UV−vis−NIR spectra and CIF files of the X-ray structures. This material is available free of charge via the Internet at http://pubs.acs.org.

■ AUTHOR INFORMATION

Corresponding Author

*Fax: +49-6226-546617. E-mail: peter.comba@aci.uni-heidelberg.de.

■ ACKNOWLEDGMENT

Financial support by the German Science Foundation (DFG) is gratefully acknowledged. We thank Dr. Christopher Noble for his contribution in incorporating the additional ZFS terms into the anisotropic exchange term of the spin Hamiltonian in the Molecular Sophe computer simulation software suite (v 2.1.6). M.A. thanks Prof. Dr. Frank Neese and the SFB 813 (Chemistry on Spin Centers) for financial support.

■ REFERENCES

(1) Guha, B. *Proc. R. Soc. London, Ser. A* **1951**, *206*, 353.
(2) Bleaney, B.; Bowers, K. D. *Proc. R. Soc. London, Ser. A* **1952**, *214*, 451.
(3) Ozarowski, A. *Inorg. Chem.* **2008**, *47*, 9760.
(4) Sharpe, A. G. *The Chemistry of Cyano Complexes of the Transition Metals*; Academic Press: New York, 1976.
(5) Atanasov, M.; Comba, P.; Daul, C. A. *J. Phys. Chem. A* **2006**, *110*, 13332.
(6) Atanasov, M.; Comba, P.; Daul, C. A. *Inorg. Chem.* **2008**, *47*, 2449.
(7) Atanasov, M.; Busche, C.; Comba, P.; El Hallak, F.; Martin, B.; Rajaraman, G.; van Slageren, J.; Wadepohl, H. *Inorg. Chem.* **2008**, *47*, 8112.
(8) Rodriguez-Fortea, A.; Alemany, P.; Alvarez, S.; Ruiz, E. *Inorg. Chem.* **2002**, *41*, 3769.
(9) Rodriguez-Fortea, A.; Alemany, P.; Alvarez, S.; Ruiz, E.; Scuiller, A.; Decroix, C.; Marvaud, V.; Vaissermann, J.; Verdaguer, M.; Rosenman, I.; Julve, M. *Inorg. Chem.* **2001**, *40*, 5868.
(10) Caneschi, A.; Gatteschi, D.; Sessoli, R.; Barra, A. L.; Brunel, L. C.; Guillot, M. *J. Am. Chem. Soc.* **1991**, *113*, 5873.
(11) Sessoli, R.; Tsai, H.-L.; Schake, A. R.; Wang, S.; Vincent, J. B.; Folting, K.; Gatteschi, D.; Christou, G.; Hendrickson, D. N. *J. Am. Chem. Soc.* **1993**, *115*, 1804.
(12) Comba, P.; Hausberg, S.; Martin, B. *J. Phys. Chem. A* **2009**, *113*, 6751.
(13) Ruiz, E.; Cauchy, T.; Cano, J.; Costa, R.; Tercero, J.; Alvarez, S. *J. Am. Chem. Soc.* **2008**, *130*, 7420.
(14) Piligkos, S.; Bill, E.; Collison, D.; McInnes, E. J. L.; Timco, G. A.; Weihe, H.; Winpenny, R. E. P.; Neese, F. *J. Am. Chem. Soc.* **2007**, *129*, 760.
(15) Sessoli, R.; Gatteschi, D. *Angew. Chem., Int. Ed.* **2003**, *42*, 268.
(16) Boca, R. *Coord. Chem. Rev.* **2004**, *248*, 757.
(17) Zein, S.; Duboc, C.; Lubitz, W.; Neese, F. *Inorg. Chem.* **2008**, *47*, 134.
(18) Comba, P.; Kerscher, M. *Coord. Chem. Rev.* **2009**, *253*, 564.
(19) Atanasov, M.; Comba, P.; Hausberg, S.; Martin, B. *Coord. Chem. Rev.* **2009**, *253*, 2306.
(20) Waldmann, O. *Inorg. Chem.* **2007**, *46*, 10035.
(21) Cirera, J.; Ruiz, E.; Alvarez, S.; Neese, F. *Chem.—Eur. J.* **2009**, *15* (16), 4078.
(22) Milios, C. J.; Vinslava, A.; Wernsdorfer, W.; Moggach, S.; Parsons, S.; Perlepes, S. P.; Christou, G.; Brechin, E. K. *J. Am. Chem . Soc.* **2007**, *129*, 2754.
(23) Ishikawa, N.; Mizuno, Y.; Takamatsu, S.; Ishikawa, T.; Koshihara, S. *Inorg. Chem.* **2008**, *47*, 10217.
(24) Comba, P.; Kerscher, M.; Schiek, W. *Prog. Inorg. Chem.* **2007**, *55*, 613.
(25) Haller, R.; Unholzer, H. *Arch. Pharm.* **1972**, *305*, 855.
(26) Börzel, H.; Comba, P.; Hagen, K. S.; Merz, M.; Lampeka, Y. D.; Lienke, A.; Linti, G.; Pritzkow, H.; Tsymbal, L. V. *Inorg. Chim. Acta* **2002**, *337*, 407.
(27) Comba, P.; Kerscher, M.; Merz, M.; Müller, V.; Pritzkow, H.; Remenyi, R.; Schiek, W.; Xiong, Y. *Chem.—Eur. J.* **2002**, *8*, 5750.
(28) Comba, P.; Hauser, A.; Kerscher, M.; Pritzkow, H. *Angew. Chem., Int. Ed.* **2003**, *42*, 4536. *Angew. Chem.* **2003**, *115*, 4675.
(29) Bentz, A.; Comba, P.; Deeth, R. J.; Kerscher, M.; Pritzkow, H.; Seibold, B.; Wadepohl, H. *Inorg. Chem.* **2008**, *47*, 9518.
(30) Banci, L.; Bencini, A.; Benelli, C.; Dei, A.; Gatteschi, D. *Inorg. Chem.* **1981**, *20*, 1399.
(31) Bencini, A.; Gatteschi, D.; Zanchini, C. *Inorg. Chem.* **1985**, *24*, 704.
(32) Bencini, A.; Gatteschi, D.; Zanchini, C. *Inorg. Chem.* **1986**, *25*, 2211.

(33) Charlot, M.-F.; Journaux, Y.; Kahn, O.; Bencini, A.; Gatteschi, D.; Zanchini, C. *Inorg. Chem.* **1986**, *25*, 1060.
(34) Ozarowski, A.; Reinen, D. *Inorg. Chem.* **1986**, *25*, 1704.
(35) Bencini, A.; Fabretti, A. C.; Yanchini, C.; Zannini, P. *Inorg. Chem.* **1987**, *26*, 1445.
(36) Bencini, A.; Gatteschi, D. *Mol. Phys.* **1982**, *47*, 161.
(37) Bencini, A.; Gatteschi, D. *EPR of Exchange Coupled Systems*; Springer-Verlag: Berlin, Germany, 1990.
(38) Atanasov, M.; Comba, P. *Structure and Function*; Comba, P., Ed.; Springer: Heidelberg, Germany, 2010; p 53.
(39) Atanasov, M.; Comba, P. *The Jahn-Teller Effect - Advances and Perspectives*; Köppel, H., Yarkony, D. R., Barentzen, H., Eds.; Springer: Heidelberg, 2009; p 621.
(40) Maurice, R.; Bastardis, R.; de Graaf, C.; Suaud, N.; Mallah, T.; Guihéry, N. *J. Chem. Theory Comput.* **2009**, *5*, 2977.
(41) Maurice, R.; Guihéry, N.; Bastardis, R.; de Graaf, C. *J. Chem. Theory Comput.* **2010**, *6*, 977.
(42) Maurice, R.; de Graaf, C.; Guihéry, N. *J. Chem. Phys.* **2010**, *133*, 084307.
(43) Orpen, A. G.; Brammer, L.; Allen, F. H.; Kennard, O.; Watson, D. G.; Taylor, R. *J. Chem. Soc., Dalton Trans.* **1989**, 1.
(44) Hay, P. J.; Thibeault, J. C.; Hoffmann, R. J. *J. Am. Chem .Soc.* **1975**, *97*, 4884.
(45) Born, K.; Comba, P.; Ferrari, R.; Kuwata, S.; Lawrance, G. A.; Wadepohl, H. *Inorg. Chem.* **2007**, *46*, 458.
(46) Bleiholder, C.; Börzel, H.; Comba, P.; Ferrari, R.; Heydt, A.; Kerscher, M.; Kuwata, S.; Laurenczy, G.; Lawrance, G. A.; Lienke, A.; Martin, B.; Merz, M.; Nuber, B.; Pritzkow, H. *Inorg. Chem.* **2005**, *44*, 8145.
(47) Dows, D. A.; Haim, A.; Wilmarth, W. K. *J. Inorg. Nucl. Chem.* **1961**, *21*, 33.
(48) Magnetic data were also collected for $[\{Ni(L^3)\}_2(CN)](BF_4)_3$. Although these have interesting features, we restrict ourselves to the discussion of the electronic properties of the Cu^{II} complexes, and $[\{Ni(L^3)\}_2(CN)](BF_4)_3$ appears only for structural comparison.
(49) This is expected for this type of dinuclear Cu^{II} complexes which usually contain between 1 and 5% mononuclear Cu^{II} species as impurities.[37] An impurity of mononuclear Cu^{II} species has been included in the Bleaney−Bowers fits of the magnetic data (see Figure 2) and was subtracted from the experimental EPR spectra to obtain the EPR spectra of the dinuclear complexes (Figures 4, Figures S3 and S4).
(50) Kahn, O. *Molecular Magnetism*; Wiley&Sons Inc.: New York, 1993.
(51) Comba, P.; Merz, M.; Pritzkow, H. *Eur. J. Inorg. Chem.* **2003**, 1711.
(52) No well enough resolved spectrum of the L^2-based mononuclear complex was obtained.
(53) Hanson, G. R.; Gates, K. E.; Noble, C. J.; Griffin, M.; Mitchell, A.; Benson, S. *J. Inorg. Biochem.* **2004**, *98*, 903.
(54) Pilbrow, J. R. *Transition Ion Electron Paramagnetic Resonance*; Clarendon Press: Oxford, U.K., 1990.
(55) Smith, T. D.; Pilbrow, J. R. *Coord. Chem. Rev.* **1974**, *13*, 173.
(56) Hanson, G. R.; Noble, C. J.; Benson, S. *High Resolution EPR: Applications to Metalloenzymes and Metals in Medicine*; Hanson, G. R., Berliner, L. J., Eds.; Springer: Dordrecht, The Netherlands, **2009**; Vol. *28*, p 105.
(57) Two additional absorption bands with maxima at approximately 23,000 and 27,000 cm^{-1} in both complexes (see Supporting Information, Figures S7 and S8) are assigned to ligand to metal charge transfer transitions.
(58) Noodleman, L. *J. Chem. Phys.* **1981**, *74*, 5737.
(59) Soda, T.; Kitagawa, Y.; Onishi, T.; Takano, Y.; Shigeta, Y.; Nagao, H.; Yoshioka, Y.; Yamaguchi, K. *Chem. Phys. Lett.* **2000**, *319*, 223.
(60) Atanasov, M.; Daul, C. A.; Rauzy, C. *Chem. Phys. Lett.* **2003**, *367*, 737.
(61) Atanasov, M.; Daul, C. A.; Rauzy, C. *Struct. Bonding (Berlin)* **2004**, *106*, 97.
(62) Atanasov, M.; Rauzy, C.; Baettig, P.; Daul, C. A. *Int. J. Quant. Chem.* **2005**, *102*, 119.
(63) Comba, P.; Hambley, T. W.; Hitchman, M. A.; Stratemeier, H. *Inorg. Chem.* **1995**, *34*, 3903.
(64) Comba, P. *Coord. Chem. Rev.* **1999**, *182*, 343.
(65) Atanasov, M.; Baerends, E. J.; Baettig, P.; Bruyndonckx, R.; Daul, C.; Rauzy, C.; Zbiri, M. *Chem. Phys. Lett.* **2004**, *399*, 433.
(66) Smith, T. D.; Pilbrow, J. R. *Coord. Chem. Rev.* **1974**, *13*, 173.
(67) Atanasov, M.; Daul, C. A.; Güdel, H. U.; Wesolowski, T. A.; Zbiri, M. *Inorg. Chem.* **2005**, *44*, 2954.
(68) Pascal, P.; Pacault, A.; Hoarau, J. *C. R. Acad. Sci.* **1951**, *233*, 1078.
(69) *SAINT*; Bruker AXS: Madison, WI, 1997−2008.
(70) Blessing, R. H. *Acta Crystallogr.* **1995**, *A51*, 33.
(71) Sheldrick, G. M. *SADABS-2004−2008, Bruker AXS, SADABS-2004/1*; Bruker AXS: Madison, WI, Göttingen, Germany, 2004−2008.
(72) Sheldrick, G. M. *SHELXS-97*; University of Göttingen: Göttingen, Germany, 1997.
(73) Sheldrick, G. M. *Acta Crystallogr.* **2008**, *A64*, 112.
(74) Beurskens, P. T. *Crystallographic Computing 3*;Sheldrick, G. M., Krüger, C., Goddard, R., Eds.; Clarendon Press: Oxford, U.K., 1985; p 216.
(75) Beurskens, P. T.; Beurskens, G.; de Gelder, R.; Smits, J. M. M.; Garcia-Granda, S.; Gould, R. O. *DIRDIF-2008*; Radboud University: Nijmegen, The Netherlands, 2008.
(76) Sheldrick, G. M. *SHELXL-97*; University of Göttingen: Göttingen, Germany, 1997.
(77) Sluis, P. v. d.; Spek, A. L. *Acta Crystallogr.* **1990**, *A46*, 194.
(78) Spek, A. L. *PLATON*; Utrecht University: Utrecht, The Netherlands: 2003.
(79) Spek, A. L. *J. Appl. Crystallogr.* **2003**, *36*, 7.
(80) Neese, F. *ORCA, an ab initio, density functional, and semiempirical program package*; Rheinische Friedrich-Wilhelms-Universtität: Bonn, Germany, 2008.
(81) Becke, A. D. *J. Chem. Phys.* **1992**, *96*, 2155.
(82) Becke, A. D. *J. Chem. Phys.* **1992**, *97*, 9713.
(83) Becke, A. D. *J. Chem. Phys. B* **1993**, *98*, 5648.
(84) Schäfer, A.; Horn, H.; Ahlrichs, R. *J. Chem. Phys.* **1992**, *97*, 2571.
(85) Schäfer, A.; Huber, C.; Ahlrichs, R. *J. Chem. Phys.* **1994**, *100*, 5829.
(86) Ditchfield, R.; Hehre, W. J.; Pople, J. A. *J. Chem. Phys.* **1971**, *54*, 724.
(87) Hehre, W. J.; Ditchfield, R.; Pople, J. A. *J. Chem. Phys.* **1972**, *56*, 2257.
(88) Hariharan, P. C.; Pople, J. A. *Mol. Phys.* **1974**, *27*, 209.
(89) Gordon, M. S. *Chem. Phys. Lett.* **1980**, *76*, 163.
(90) Hariharan, P. C.; Pople, J. A. *J. Chem. Phys.* **1973**, *82*, 213.
(91) Blaudeau, J.-P.; McGrath, M. P.; Curtiss, L. A.; Radom, L. *J. Chem. Phys.* **1997**, *107*, 5016.
(92) Francl, M. M.; Pietro, W. J.; Hehre, W. J.; Binkley, J. S.; DeFrees, D. J.; Pople, J. A.; Gordon, M. S. *J. Chem. Phys.* **1982**, *77*, 3654.
(93) Binning, R. C., Jr.; Curtiss, L. A. *J. Comput. Chem.* **1990**, *11*, 1206.
(94) Rassolov, V. A.; Pople, J. A.; Ratner, M. A.; Windus, T. L. *J. Chem. Phys.* **1998**, *109*, 1223.
(95) Rassolov, V. A.; Ratner, M. A.; Pople, J. A.; Redfern, P. C.; Curtiss, L. A. *J. Comput. Chem.* **2001**, *22*, 976.
(96) Adamsky, H. *(with contributions from P.E. Hoggard, M. Atanasov, and K. Eifert) AOMX − angular overlap model program, available free of charge from the internet at* http://www.aomx.de.
(97) *Matlab 7.5.0 (R2007b), MathWorks. Copies of the programs can be obtained from mihail.atanasov@aci.uni-heidelberg.de.*
(98) Merz, K. W.; Haller, R. *Pharm. Acta Helv.* **1963**, *38*, 442.
(99) Caujolle, R.; Castera, P.; Lattes, A. *Bull. Soc. Chim. Fr.* **1984**, *9−10*, 413.
(100) Börzel, H.; Comba, P.; Hagen, K. S.; Katsichtis, C.; Pritzkow, H. *Chem.—Eur. J.* **2000**, *6*, 914.
(101) Börzel, H.; Comba, P.; Hagen, K. S.; Kerscher, M.; Pritzkow, H.; Schatz, M.; Schindler, S.; Walter, O. *Inorg. Chem.* **2002**, *41*, 5440.